Global structure and dynamics of large-scale fluctuations in the solar wind: Voyager 2 observations during 2005 and 2006

L. F. Burlaga,[1] N. F Ness,[2] M. H. Acũna,[3] Y.-M. Wang,[4] N. R. Sheeley Jr.,[4] C. Wang,[5] and J. D. Richardson[6]

Received 5 September 2007; revised 24 October 2007; accepted 20 November 2007; published 22 February 2008.

[1] The Voyager 2 (V2) observations of daily averages of the solar wind during 2005 and 2006 from 75.3 AU to 81.6 AU between ≈25.7°S and 27.1°S show both a step-like trend in the speed V(t) and "large-scale fluctuations" of the magnetic field strength B, speed V, density N and temperature T. The distribution functions of B, N, and NV^2 observed by V2 are lognormal and that of V is approximately Gaussian. We introduce a method for specifying the boundary conditions at all latitudes (except near the poles) on a Sun-centered surface of radius of 1 AU, based on solar magnetic field observations. This paper uses only the boundary conditions at the latitude of V2 and a 1-D time-dependent MHD model to calculate the radial evolution of the large-scale fluctuations of B(t), V(t) and N(t) at distances between 1 and 90 AU. This model explains the V2 observations of a lognormal distribution of B and the Gaussian distribution of V, but not the observed lognormal distributions of N and NV^2. The lognormal distribution of B observed by V2 was produced primarily by dynamical processes beyond 1 AU.

Citation: Burlaga, L. F., N. F. Ness, M. H. Acũna, Y.-M. Wang, N. R. Sheeley Jr., C. Wang, and J. D. Richardson (2008), Global structure and dynamics of large-scale fluctuations in the solar wind: Voyager 2 observations during 2005 and 2006, *J. Geophys. Res.*, *113*, A02104, doi:10.1029/2007JA012796.

1. Introduction

[2] This paper analyzes the temporal profiles of the magnetic field strength B, solar wind speed V, proton density N, and proton temperature T observed by Voyager 2 (V2) in the supersonic solar wind during 2005 and 2006 at distances from 75.3 AU to 81.6 AU and latitudes between 25.7°S and 27.1°S. Both the trend of V(t) and the large-scale fluctuations about this trend are examined, with emphasis on the latter. We provide an explanation of these results using a model for the radial evolution of the profiles of B(t), V(t), N(t) and T(t).

[3] "Large-scale fluctuations" in the magnetic field and plasma in the solar wind are defined as variations of B, V, N, and T observed by a spacecraft on scales ranging from ≈1 day to several solar rotations, which can be seen in time series of the order of 1 year [*Burlaga and Mish*, 1987; *Burlaga et al.*, 1987, 1989]. At 1 AU these fluctuations are typically associated with the collective properties of streams, interaction regions, ejecta as well as the internal structure of these components [*Hundhausen*, 1972; *Burlaga*, 1995]. At larger distances from the Sun, the flows evolve and interact such that new larger features appear, such as Merged Interaction Regions (MIRs) [*Burlaga*, 1984, 1995]. In general, the multiscale fluctuations observed during a year are complex, and they can only be described statistically.

[4] Modeling large-scale fluctuations at various positions in the heliosphere between 1 and ≈100 AU requires the specification of at least V, N, T and B as a function of time on some inner boundary, such as a Sun-centered sphere at 1 AU. Since the boundary conditions are as important as the equations in any model of the temporal variations of B, V, N, and T throughout the heliosphere, the boundary conditions are discussed at length in section 3. We use the term 'model' to include both the boundary conditions and the equations.

[5] During the period 2004 and 2005 considered in this paper, the solar cycle was in its declining phase. Latitudinal gradients can be significant during this phase [*Schwenn et al.*, 1978]. Thus one should use boundary conditions at ≈26°S and 1 AU to model the V2 observations discussed in section 2. Since there are no spacecraft at ≈26°S near 1 AU, section 3 introduces a new method for determining the boundary conditions on a Sun-centered spherical surface with a radius of 1 AU (hereafter called "our solar boundary conditions").

[6] The radial evolution of B(t), V(t), N(t) between 1 AU and 90 AU, predicted by a 1-D time-dependent MHD model and our solar boundary conditions, is discussed in section 5. These results are qualitatively similar to those found previously using boundary conditions provided by the WIND plasma and magnetic field data [*Ogilvie et al.*, 1995, and

[1]NASA/Goddard Space Flight Center, Geospace Physics Laboratory, Greenbelt, Maryland, USA.
[2]Institute for Astrophysics and Computational Sciences, Catholic University of America, Washington DC, USA.
[3]Solar System Exploration Division, NASA Goddard Space Flight Center, Greenbelt, Maryland, USA.
[4]Naval Research Laboratory, Washington DC, USA.
[5]State Key Laboratory of Space Weather, Center for Space Science and Applied Research, Chinese Academy of Science, Beijing, China.
[6]Kavli Institute for Astrophysics and Space Research, Massachusetts Institute of Technology, Cambridge, Massachusetts, USA.

Copyright 2008 by the American Geophysical Union.
0148-0227/08/2007JA012796

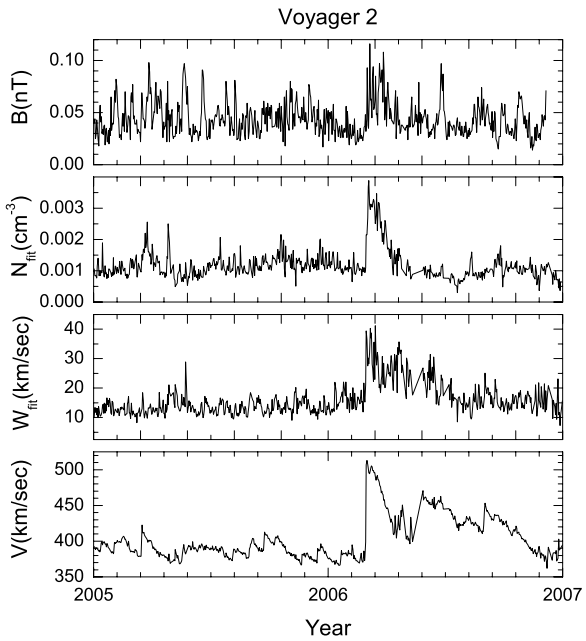

Figure 1. Voyager 2 observations of daily averages of magnetic field strength B, density N_{fit}, proton thermal speed W_{fit}, and bulk speed V.

Lepping et al., 1995, respectively], which we shall refer to as "the WIND 1995 boundary conditions". These boundary conditions were used to describe the evolution of corotating streams [*Hundhausen*, 1972, 1977] observed in 1995 [*Burlaga et al.*, 2003a, 2003b]. The WIND 1995 boundary conditions (in the ecliptic) are more accurate and have higher resolution than those on a sphere that are derived from our solar boundary conditions. However, the latter allow one to predict properties of the large-scale fluctuations at the latitude of V2. It would be straightforward to repeat the calculations described in this paper for a broad range of latitudes and thereby derive a 3-D description of the radial evolution of large-scale fluctuations throughout the heliosphere for the declining phase of the solar cycle. However, it would be feasible and preferable to use a 3-D MHD model to derive the 3-D description of the radial evolution of the large-scale fluctuations.

[7] This paper demonstrates the feasibility and potential of using solar observations to provide the boundary conditions needed to model the basic characteristics of V2 observations of B(t) and V(t). Since we assume that B = constant at 1 AU, the paper also shows that the fluctuations in B observed by V2 were produced primarily by dynamical processes beyond 1 AU. The probability distribution function ("pdf") of the fluctuations in N observed by V2 was not predicted by the model, probably owing to the limitations of our solar boundary conditions. It should be possible to greatly improve the specification of the 3-D boundary conditions at 1 AU in the next decade or so.

2. Voyager 2 Observations of the Magnetic Field and Plasma During 2005 and 2006

[8] Figure 1 shows daily averages of B(t) from the magnetic field experiment on V2 [*Behannon et al.*, 1977], as well as the density (N_{fit}) and thermal speed (W_{fit}) and bulk speed V derived from fits of the observed velocity distributions from the plasma experiment on V2 [*Bridge et al.*, 1977] from 2005 through 2006. The data show a large enhancement in B, V, N, and T beginning abruptly at a shock between days 59 and 60, 2006 and extending for at least 40 days thereafter. This transient feature was identified by [*Richardson et al.*, 2006] as a MIR. Since transient flows are not considered in our solar boundary conditions, and since the event was already analyzed in detail, it will not be considered further in this paper. The transient flow was followed by an extended high-speed flow from ~DOY 100 to ~300, 2006. The basic trend in the speed profile observed by V2 during 2005 and 2006 is described in section 4, where it is compared with the prediction.

[9] The fluctuations in B, V, and N observed by V2 during 2005 were relatively homogeneous (Figure 1). Therefore we use these data in our discussion of the large-scale fluctuations of B, V, and N observed by V2. One quantitative measure of these large-scale fluctuations is provided by the corresponding probability distributions. Figures 2a, 2b, and 2c shows the probability distributions of $\log(B/\langle B\rangle)$, V, and log(N), respectively, that were observed by V2 during 2005. Since the distribution of $\log(NV^2)$ is particularly important in determining the position of the heliopause and termination shock [e.g., *Richardson and Wang*, 2005(as is the distribution of V itself [*Whang et al.*, 2003]), this distribution is also shown, in Figure 2d.

[11] The curves in Figure 2 are fits of the data to a Gaussian distribution, $y = y_o + A/[w \times (\pi/2)] \times \exp[-2[(x - x_c)/w]^2$. The distribution of $x = \log(B/\langle B\rangle)$ observed by V2 during 2005 between 75.3 and 78.4 AU is Gaussian, indicating a lognormal distribution of $B/\langle B\rangle$, consistent with previous observations of the distributions of B throughout the heliosphere [*Burlaga*, 2001]. Both N and NV^2 observed by V2 during 2005 also have lognormal distributions. The distribution of V is consistent with a Gaussian distribution within the uncertainties, but a lognormal distribution of V is also consistent with the observations. The parameters of the Gaussian fits to the observations of $\log(B/\langle B\rangle)$, V, log(N) and $\log(NV^2)$ are shown in Figure 2.

3. Boundary Conditions at 1 AU

3.1. General Remarks

[12] In order to predict the temporal profiles of V(t; R), B(t; R), N(t; R), and T(t; R) of the supersonic solar wind at a spacecraft beyond 1 AU, it is necessary to specify conditions at some inner boundary at $\leq$1 AU as a function of time, since the basic equations describing the evolution are hyperbolic. Most previous models of solar wind flows used data from one spacecraft to predict what would be observed at another spacecraft that is farther from the Sun. This approach is fruitful when the radial, latitudinal and longitudinal separations between the spacecraft are small [see, e.g., the references in *Hundhausen*, 1972; *Burlaga et al.*, 1985, and *Burlaga et al.*, 2005]. When the radial separation of the two spacecraft is large and the time interval considered is very short, as when considering a shock or a single transient flow, it is still possible to predict the time series measured by a distant spacecraft using boundary conditions provided by a spacecraft closer to the Sun [see, e.g., *Wang et al.*, 2001, *Whang et al.*, 2001, and *Burlaga et al.*, 2001].

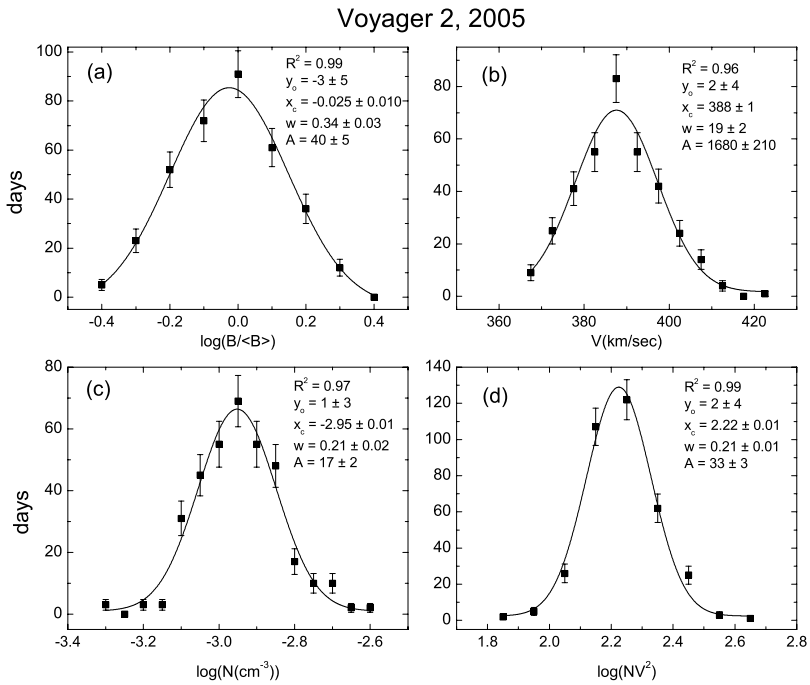

Figure 2. The points show histograms of (a) $\log(B/\langle B\rangle)$, (b) V, (c) log(N), and (d) $\log(NV^2)$ based on daily averages of B, V, and N observed by Voyager 2 during 2005. The curves are least fits to the normal distribution with the parameters shown.

[13] When the radial separation of the two spacecraft is large and the time interval is large (e.g., 6 months or more), it is not possible to propagate the results from 1 spacecraft (e.g., WIND at 1 AU) to another, because the inner spacecraft rotates more rapidly about the Sun than the outer spacecraft, in accordance with Kepler's law. For example, when Voyager is beyond ≈50 AU, its azimuthal displacement is very small during 6 months, whereas in the same period WIND moves 180° around the Sun; there can be no approximate co-alignment throughout the period. Thus it is generally not possible to predict the detailed time series at a distant spacecraft such as V1 and V2 using input data from a single spacecraft such as WIND or ACE (Advanced Composition Explorer).

[14] *Burlaga et al.* [2003a, 2003b, 2003c] showed that one can describe the large-scale fluctuations at any point in the heliosphere by specifying the statistical state as a function of scale. They showed also that this statistical state can be predicted with a deterministic MHD model using boundary conditions given by observations from a single spacecraft at 1 AU. One regards the time series (e.g., B(t) and V(t)) predicted at a given distance R from the Sun as a representative sample of conditions at that distance. In this way one can predict, as a function of distance and scale, the observed probability density functions and spectra [*Burlaga et al.*, 2003a, 2003b, 2003c], and the multifractal structure [*Burlaga et al.*, 2003d]. One can also predict the distribution of increments of B(t) (which can be described by the Tsallis distribution of nonextensive statistical mechanics) from 5 to 90 AU on scales from 1 day to 128 days [*Burlaga et al.*, 2007].

[15] When the latitude of the inner spacecraft (which provides the boundary conditions) differs significantly from that of the more distant spacecraft, it is not even possible to predict the statistical state of the solar wind at the more distant spacecraft. Ultimately, global boundary conditions are needed to predict the time profiles of the MHD quantities at any point in the 3-D global heliosphere, i.e., it is necessary to provide B(t), V(t), N(t) and T(t) everywhere on a closed surface centered at the Sun with a radius ≤1 AU. Such boundary conditions on the surface can only be determined from global observations of the Sun.

[16] It is possible to predict the speed profiles at WIND, ACE and Ulysses in some average sense from observations of the solar magnetic field. For example, *Whang et al.* [2005] computed the global structure of the speed from 1968 through 2003 and compared these speeds with Ulysses observations of the latitudinal variations near solar minimum. Similarly, *Wang and Sheeley* [2006] considered the projection of the Ulysses trajectory and showed that the temporal variations of the observed speeds (which depend on a wide range of latitudes and a relatively small range of radial distances) for various Carrington rotations show the same pattern as the speeds computed from the flux tube divergence factors. However, at present, solar observations are made from near-Earth, where only half the Sun is observed at any time. *Wang and Sheeley* [2006] published a map of speed as a function of latitude and longitude versus time, derived from solar magnetic field observations. This type of map is the starting point for our method of specifying the inner boundary conditions, described in the next section.

3.2. 3-D Boundary Conditions at 1 AU: A First Approximation

3.2.1. Speeds on the Inner Boundary

[17] The bulk speed of solar wind protons at Earth is inversely correlated with the rate of flux tube divergence near the Sun: the higher the solar wind speed, the more

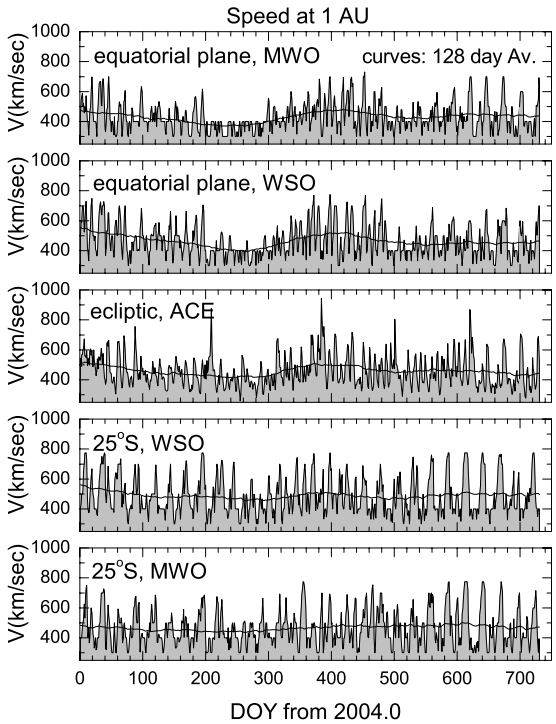

Figure 3. The solar wind speed at 1 AU inferred from Mount Wilson Observatory (MWO) and Wilcox Solar Observatory (WSO) in the solar equatorial plane, measured in situ in the ecliptic by ACE, and inferred from WSO and MWO at 25.5°S.

slowly the associated coronal flux tube expands [see *Levine et al.*, 1977; *Wang and Sheeley*, 1990; *Wang et al.*, 1997; *Arge and Pizzo*, 2000; *Poduval and Zhao*, 2004; *Whang et al.*, 2005].

[18] In the PFSS (Potential Field Source Surface) model, the coronal magnetic field is computed using a potential magnetic field model between the Sun (where the radial component of the potential field is matched to the observed magnetic field [*Wang and Sheeley*, 1992] and the outer boundary ("source surface") at ≈2.5 solar radii where the magnetic field is assumed to be radial [*Schatten et al.*, 1969, *Wang and Sheeley*, 1992]. The flux tube divergence is computed by determining the ratio of the solid angle between its foot point location and the "source surface". The speed is then determined from the flux tube divergence [*Wang and Sheeley*, 1990]. Several papers discuss the comparison of the predictions with this model with observations [*Wang and Sheeley*, 2006; *Whang et al.*, 2005; *Sheeley et al.*, 1997; and *Wang et al.*, 1997].

[19] *Wang and Sheeley* [2006] calculated the solar wind speeds as a function of latitude for each Carrington rotation from 1991 to 2006. Given such a plot for a given distance, say 1 AU, one can compute speed as a function of time for any curve on the boundary surface, which can be the projection of a spacecraft trajectory for example. Thus it is possible to calculate the approximate speeds as a function of latitude and time on a Sun-centered surface with a radius of 1 AU that can serve as one of the inner boundary conditions for a 3-D model of the heliosphere. There is some ambiguity in longitude, since the model determines speeds for successive Carrington Rotations, which are related to the position of Earth, whereas one would like to have the speeds relative to an inertial system. This limitation could be removed in the future if observations of the 'backside' of the sun, become available.

[20] This paper considers the speeds computed from the flux tube expansion factors determined using the Mount Wilson Observatory observations of the photospheric magnetic field during 2004 and 2005. During the corresponding interval at V2 (the propagation time of the solar wind from 1 AU to the distance of V2 in 2005–2006 is nearly a year), the latitude of V2 was between 25.7°S and 27.1°S. We determined the boundary condition for the speed profile at 25.5°S and 1 AU, obtained from the solar observations as discussed above. The speed was corrected in a rough way for interactions between fast and slow solar wind between the Sun and 1 AU by averaging neighboring pixels, but a dynamical model that would account for nonlinear effects such as stream steepening was not used.

[21] In order to examine the latitude gradients at 1 AU during 2004 and 2005, we compare the speed profiles predicted near the equatorial plane with those near ≈25.5°S. The top two panels in Figure 3 show the speed profiles in the solar equatorial plane derived using the solar magnetic field data from the Mount Wilson Observatory (MWO) and the Wilcox Solar Observatory (WSO), respectively, together with the speed measured by ACE [*McComas et al.*, 1998] in the ecliptic plane during 2004 and 2005. Although there are differences in detail, the basic features of the fluctuations are the same in all three panels. Similarly, the bottom two panels in Figure 3 show the speed profiles derived from the WSO and MWO data at ≈25.5°S. Again, there are differences in detail, but the basic features of the fluctuations in V(t) are the same in these two cases. However, the fluctuations at ≈25.5°S differ from those at and near the ecliptic. The recurrent streams at ≈25.5°S have larger amplitudes and a more periodic structure than the streams observed near the solar equatorial plane. Thus the latitude variations of V(t) are significant at the inner boundary, and it is more appropriate to use the profiles at ≈25.5°S as input to a model for the observations of V2 (which was at ≈26°S in the corresponding interval under consideration) than the in situ observations from ACE in the ecliptic.

3.2.2. N, T, and B on the Inner Boundary

[22] For any time-dependent MHD model of the 3-D solar wind, one needs B(t), N(t), T(t), as well as V(t) on the inner boundary. However, it is not yet possible to obtain maps of temporal variations of N, T, and B on the inner boundary surface at 1 AU from solar observations, corresponding to those for V described above. Thus we use an indirect method to estimate N(t), T(t), and B(t) at 1 AU and ≈25.5°S. This method provides a first approximation to the boundary conditions.

[23] The proton temperature is high and the density is low in corotating streams [*Neugebauer and Snyder*, 1966]. A mathematical relationship between the density and speed and between the temperature and speed was derived by *Burlaga and Ogilvie* [1970a, 1970b], respectively; similar relationships have been found and reported by others [see, e.g., *Lopez and Freeman*, 1986]. Figure 4a shows the relationship between daily observations of T and V ob-

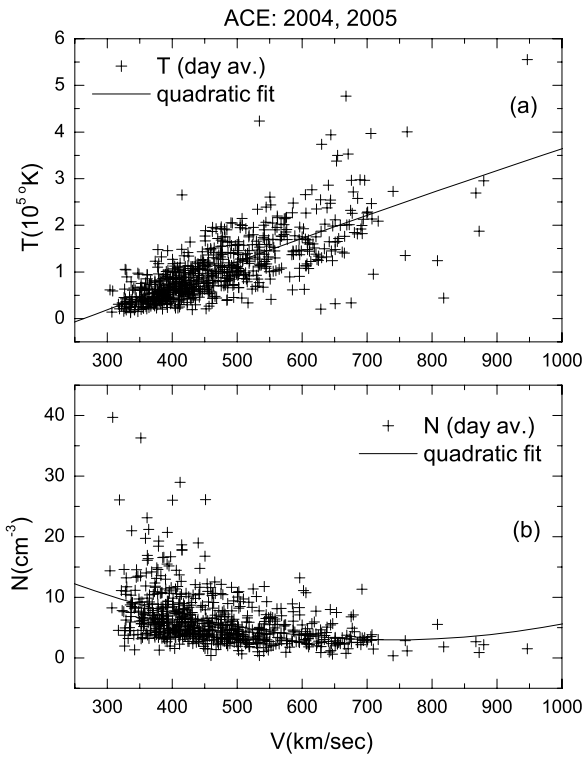

Figure 4. (a) Observations of proton temperature and speed observed by ACE during 2004 and 2005, and a quadratic fit to the observations. (b) Observations of proton density and speed observed by ACE during 2004 and 2005, and a quadratic fit to the observations.

served by ACE from 2004.0 through 2005. A quadric fit gives the relationship

$$T = -(142,000 \pm 32,000) + (550 \pm 130)V - (0.04 \pm 0.12)V^2 \quad (1)$$

for this interval. Figure 4b shows the relationship between daily observations of N and V observed by ACE from 2004.0 through 2005, and a quadric fit gives the relationship

$$N = (24.1 \pm 2.7) - (0.06 \pm 0.01)V + (3.9 \pm 0.1) \times 10^{-5} V^2 \quad (2)$$

[24] There is large scatter at the high-speed end in Figure 4a and at low speed end in Figure 4b. These deviations contribute to the discrepancies in the final results discussed below. Nevertheless, equations (1) and (2) provide a reasonable first approximation for the boundary condition at 1 AU, which is adequate for this study. We use the N(t) and T(t) profiles derived from the speed profile V(t) at ≈25.5°S obtained from MWO data, shown at the bottom of Figure 3, as inner boundary conditions for a MHD model of the radial variations of large-scale fluctuations in V, N and T between 1 AU and 100 AU at that latitude.

[25] Since the magnetic field strength is not strongly correlated with speed, we assume that B is constant at 1 AU (and at ≈25.5°S) during 2004 and 2005. This neglect of fluctuations in B at 1 AU implies that the fluctuations of B(t) that are predicted between 1 and 100 AU (section 5) arise entirely from dynamical processes in that region.

[26] The boundary conditions determined as described above are shown in Figure 5. Clearly, the assumptions we adopted to determine the boundary conditions for V, N, T, and B at 1 AU (our solar boundary conditions) give only a first approximation to the actual conditions on the inner boundary. Nevertheless, the results in sections 4 and 5 show that even this simple approximation can describe some statistical properties of the large-scale fluctuations as well as trends in the speed profile between ≈5 and 90 AU.

4. Predictions of the Speed Profile and Distributions of B, V, and N at V2

[27] We adopt the 1-D time-dependent supersonic MHD model with pickup protons [*Holzer*, 1972] introduced by C. Wang [*Wang and Richardson*, 2001a, 2001b]. Following the approach of the work by *Isenberg* [1986], the model assumes the solar wind consists of three perfectly co-moving particle populations: solar wind protons, pickup ions, and electrons. Each population is assumed to be thermalized. Unlike the three-fluid model developed by *Isenberg* [1986], which does not take into account the thermal coupling between the solar wind protons and

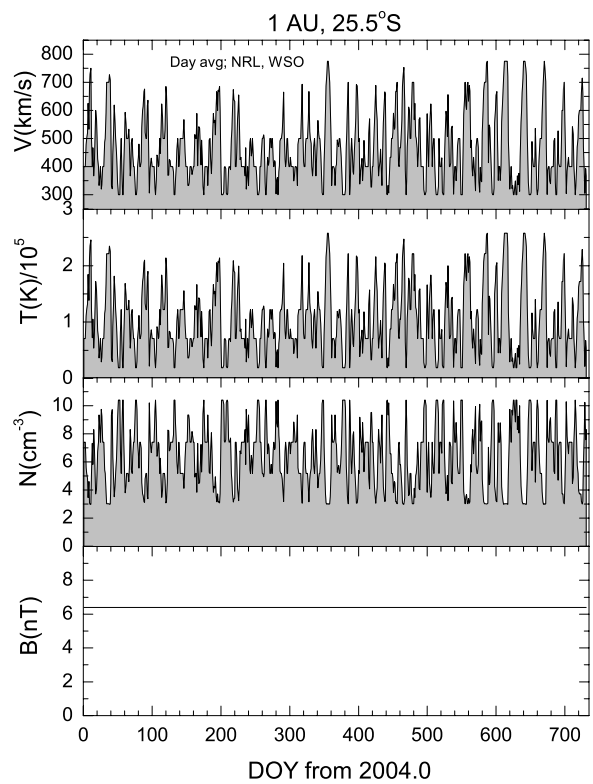

Figure 5. Our solar boundary conditions at 1 AU at 25.5°S versus day of year (DOY) measured from 2004.0. The speed V was inferred from WSO solar observations. The temperature (T) and density (N) were determined from V using the fits shown in Figures 4a and 4b, respectively. The magnetic field strength B is assumed to be constant at 1 AU throughout the interval.

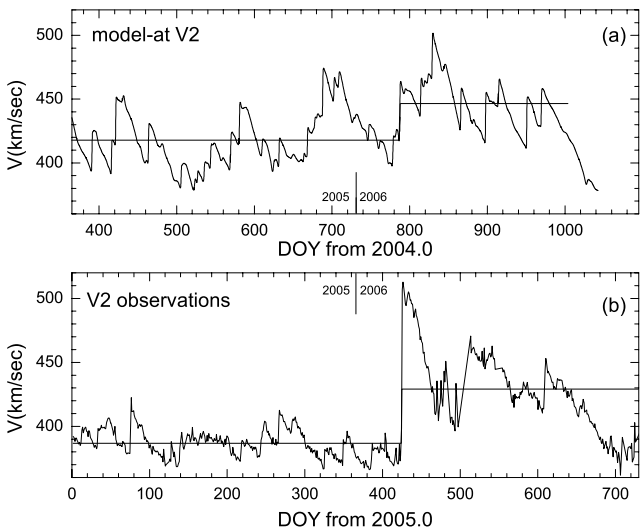

Figure 6. (a) The speed profile predicted at the position of Voyager 2 versus DOY from 2004.0. (b) The speed profile observed by Voyager 2 versus DOY from 2005.0. The curves (straight lines) in the two panels are fits to the data, as described in the text.

pickup ions, the model of Chi Wang introduces an adjustable parameter, the energy partition ratio, to predict the division of total energy provided by the pickup process between the solar wind protons and pickup ions without consideration for the details of the actual dissipation mechanism. In numerical tests, the energy partition ratio 0.05 gives the best fit to the observed proton temperature profile. This value was used in all the calculations.

[28] The predicted speed profile at the distances of V2 during 2005 and 2006 determined from our solar boundary conditions and the equations of C. Wang is shown in Figure 6a where time is measured in DOY from 2004.0. The corresponding speed profile observed by V2 is shown in Figure 6b, where time is DOY from 2005.0. Although the origin of time is different in the two panels of Figure 6, the time intervals are the same, and the data may be compared directly; the boundary between 2005 and 2006 is indicated in both panels. Note that the high speeds observed from DOY 60 to ~100, 2006 are associated with a transient flow system, as discussed above, which is not accounted for in our solar boundary conditions. This region is excluded in comparing the observed profile with the predicted profile.

4.1. Average Speed Profile

[29] The "step functions" in Figures 6a and 6b are actually fits of the predicted and observed speed profiles, respectively, to the function

$$V = V_2 + (V_1 - V_2)/[1 + \exp((t - t_o)/\tau)] \qquad (3)$$

[30] The parameters for the fit to the model are V_1 = 417.8 ± 0.3 km/s, V_2 = 446.6 ± 0.4 km/s, t_o = 787.1 ± 0.2 days, and τ = 0.2 ± 0.2 days; the square of the multiple correlation coefficient of the fit is R^2 = 0.31. The parameters for the fit to the V2 data are V_1 = 386.7 ± 1.0 km/s, V_2 = 429.1 ± 1.3 km/s, t_o = DOY 424.5 days measured from 2005.0 (DOY 59.5, 2006), and τ = 0.01 days, with R^2 = 0.49. The fitting curve to the predictions gives an abrupt jump in average speeds from 418 km/s to 447 km/s at t_o = DOY 787.1 = DOY 421.1 from 2004.0 (DOY 56, 2006), an increase of 29 km/s or 7%. Voyager 2 observed an increase in average speeds from 387 km/s to 429 km/s between days 59 and 60, 2006, an increase of 42 km/s or 11%. Thus the existence of the observed jump in V is predicted (within 4 days), but the predicted jump is 4% lower than that observed. Similarly, the speed predicted before the jump is 7.4% larger than the speed observed by V2 before the jump. Relatively high speeds are also predicted at the time the transient flow moved past V2, suggesting that the transient flow might have been 'riding on' a relatively fast flow.

[31] The variations of V(t) observed by V2 have a "jump-ramp" character, with relatively abrupt increases in V followed for several days by more slowly decreasing values of V. The model does not predict the day-to-day variations of speed profile observed by V2 exactly, because our solar boundary conditions do not specify the conditions at the longitude of V2. Nevertheless, the model does predict the jump-ramp character of the speed profile that was observed by V2. The qualitative character of fluctuations in speed observed by V2 on scales from a few days to several solar rotations is also predicted. On the other hand, the amplitudes of the predicted fluctuations (Figure 6a) appear to be somewhat larger than observed (Figure 6b), as confirmed in section 4.2.

[32] The differences between the observed and predicted average speeds and speed jump are significant. The differences between the observed and predicted amplitudes of the speed fluctuations are also significant. These differences could be due to a number of factors, including limitations of our solar boundary conditions. Such limitations can be removed in future studies. For example, better methods of providing more accurate solar boundary conditions and modeling the 3-D evolution of the flows from the Sun could be developed. The important point is that even our simple boundary conditions and equations predict the qualitative character of the speed profile observed by V2 at ≈78 AU to first approximation. This result provides a motivation and justification for the investment of time and money to obtain better observations and develop or apply more advanced models in order to remove some of the assumptions and approximations used in this paper.

4.2. Probability Distribution Functions of B, V, and N at Voyager 2

[33] The probability distributions of $\log(B/\langle B\rangle)$, V, log(N), and $\log(NV^2)$, respectively, that were predicted by the model at the location of V2 during 2005 are shown by the points and error bars in Figures 7a, 7b, 7c, and 7d, respectively. The predicted distributions of $\log(B/\langle B\rangle$ and V are Gaussian distributions (shown by the curves in Figures 7a and 7b, which are least squares fits to the predicted points), as observed by V2 (Figures 2a and 2b). It is significant that our simple solar boundary conditions and equations do not predict the Gaussian form of the corresponding distributions of log(N) and $\log(NV^2)$ observed by V2 (Figures 2c and 2d).

[35] The standard deviation (SD) of the predicted distribution of $\log(B/\langle B\rangle)$ is w/2 = 0.15 nT, consistent with that

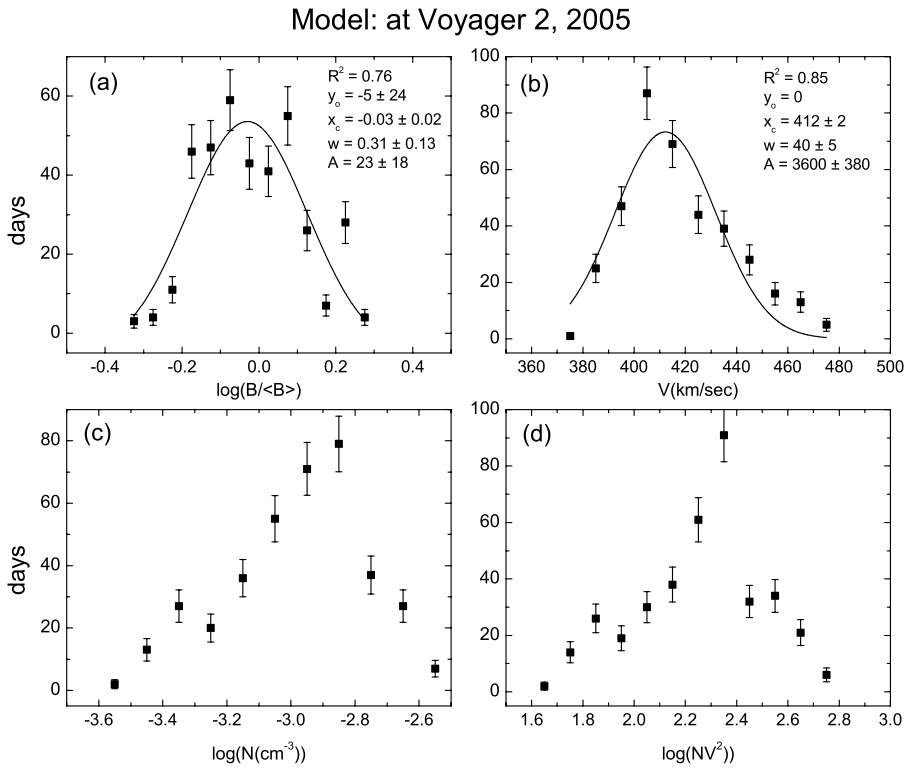

Figure 7. The points show histograms of (a) log(B/⟨B⟩), (b) V, (c) log(N), and (d) log(NV^2) based on the predicted daily averages of B, V, and N at Voyager 2 during 2005. The curves are least fits to the normal distribution with the parameters shown.

of the distribution observed by V2 during 2005 (0.13 nT). However, the SD of the predicted distribution of V (20 ± 3 km/s) is significantly broader than that observed (10 ± 2 km/s). This result is a quantitative expression of the observation made above in reference to Figure 7, that the amplitudes of the predicted fluctuations in V(t) appear to be larger than those of the observed fluctuations.

[36] The predicted distributions of log(N) and log(NV^2) shown in Figures 7c and 7d are not Gaussian, in contrast with the Gaussian distributions observed by V2. This result might reflect the inadequacy of our assumption that N(t) on the inner boundary at 1 AU can be derived from the speed there using a polynomial relation between N and V. As discussed above, the scatter of the densities observed by ACE at 1 AU relative to that predicted by a quadratic fit to the observations of N versus V is large. The neglect of this large scatter of N in our choice of N(t) at the inner boundary might be the primary reason that the model fails to predict the Gaussian distributions of log(N) and log(NV^2) observed by V2 during 2005. However, one cannot exclude the role of other approximations in contributing to the discrepancy between the predicted observed distributions involving N.

5. Predicted Radial Variation of V(t) and B(t)

[37] Given the relative success of the model in predicting the qualitative form of the observations of V(t) and B(t) and their distributions observed by V2 between 75.3 and 81.6 AU, we now consider the radial evolution of the profiles of V(t) and B(t) that are predicted by the equations of C. Wang with our solar boundary conditions. Since our solar boundary conditions depend on V, which was computed from 3-D solar observations, it is possible to compute the radial variation of V and B for each of a broad range of latitudes and thereby build a 3-D model of the large-scale fluctuations in V and B. However, our aim is to examine the feasibility of obtaining the statistical properties in the fluctuations in V and B at large distances from the sun. For this purpose it is sufficient to consider computations with our solar boundary conditions at the particular latitude of 25.5°S, corresponding to the latitude of V2 during 2005.

5.1. V(t) Versus R

[38] The profiles of V(t) were calculated at 5, 10, 15, . . ., 90 AU. A subset of these profiles (at 5, 10, 15, 20, 25, 50, 70, and 90 AU) suffices to illustrate the basic features of the radial evolution of V(t); these profiles are shown in Figure 8. Fast recurrent streams persist to 5 AU (although pairs of streams tend to merge, increasing the separation between successive streams as they move from 1 to 5 AU as discussed below). The amplitudes of the streams drop rapidly between 5 and 10 AU. A sawtooth profile in V(t), related to the formation and merging of shocks [*Burlaga et al.*, 1985, *Whang and Burlaga*, 1985, 1988; *Whang*, 1991; *Zank and Pauls*, 1997; *Rice and Zank*, 1999, *Zank*, 1999], is clearly present at 15 AU and beyond. The speed fluctuations damp slowly between 10 and 25 AU. At 50 AU the amplitudes of the speed fluctuations are small and there is little evolution between 50 and 90 AU; the solar wind is in a meta-equilibrium state there. The solar wind is never in true equilibrium, even at 90 AU, since the jump-ramp structure persists to this distance.

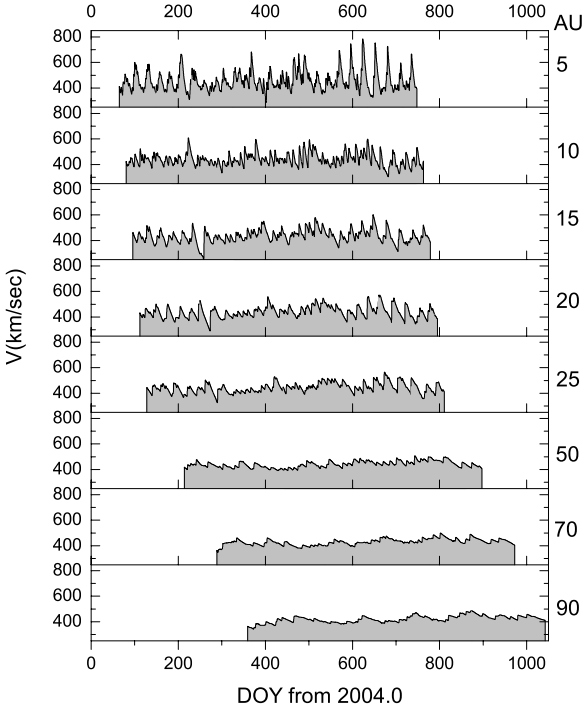

Figure 8. Predicted speed profiles from 5 to 90 AU.

[39] Figure 8 also suggests the presence of a long period (>100 day) component in the variation of V(t) at 90 AU. This component is actually a remnant of such a component that was present in the initial conditions (see Figure 1) that damped very slowly. The significance of this component will not be pursued further in this paper. Since the speed variations at 1 AU were computed from solar magnetic field observations, they must be related to features in the solar magnetic field, but the specific origin of this component is beyond the scope of this paper.

5.2. B(t) Versus R

[40] The profiles of B(t) were calculated at 5, 10, 15, . 85, and 90 AU. A subset of these profiles (at 5, 10, 15, 20, 25, 50, 70, and 90 AU) was selected to illustrate the radial evolution of B(t); these profiles are shown in Figure 9. Large-amplitude fluctuations in B (a series of MIRs) are predicted at 5 AU, despite the fact that we assumed a constant magnetic field strength at 1 AU. The large-amplitude fluctuations in B at 5 AU were produced by the steepening of the streams that were present at 1 AU, and they grew further by the merging of neighboring interaction regions. The large-scale fluctuations in B damp rapidly between 5 and 20 AU. Beyond 20 AU the MIRs gradually loose their identity.

[42] Between 50 and 90 AU the dominant fluctuations in B have periods exceeding 100 days. These fluctuations are related to similar fluctuations in V between 50 and 90 AU, and are they positively correlated with similar fluctuations predicted for N. Such fluctuations were found in V2 data by *Richardson et al.* [2003], but they not present in the V2 data considered here. The very long-period fluctuations in B were not present at 1 AU, because we assumed a constant B at 1 AU. The fluctuations in B predicted beyond 1 AU were evidently produced dynamically by the corresponding very long period fluctuations in V introduced at 1 AU.

5.3. Radial Evolution of the Spectra of V and B

[43] The spectrum of the speed variations V(t) on the inner boundary at 1 AU and 25.5°S, derived from the solar magnetic field observations for 2004 and 2005, is shown in Figure 10. Since the spectra were derived using the FFT, which uses intervals of 2^n days (n is an integer), Figures 10a and 10b show the spectra for DOY 1–512 and 215–729, respectively, measured from DOY 1, 2004. Both spectra show two peaks of essentially the same magnitude. One peak is at the solar rotation period (27 days) and the other is at ≈13.5 days (corresponding to two streams per solar rotation). Thus the principal flows considered in this paper are recurrent corotating streams, as expected for the declining phase of solar activity in solar cycle 23. The streams are related to equatorial extensions of the polar coronal holes, which rotate with the Sun [*Hundhausen*, 1977]. Since we assumed a constant magnetic field strength at 1 AU, there is no power (hence no peaks) in the spectrum of B at 1 AU.

[44] As discussed in sections 5.1 and 5.2, there was rapid evolution of the streams and magnetic field strength profiles, respectively, between 1 AU and 15 AU. The left and right columns of Figure 11 show the radial evolution of the spectra of V(t) and B(t), respectively, between 5 and 20 AU.

[46] At 5 AU, the spectrum of V shows a single strong peak at ≈26 days and only a weak remnant of a peak at 13 days, in contrast to the spectrum of V at the inner boundary at 1 AU, which shows two equally strong spectral peaks, at ≈27 and ≈13.5 days (Figure 11). The spectral change indicates that neighboring pairs of streams at 1 AU merged to form compound corotating streams between 1 and 5 AU. The compound streams damped out almost com-

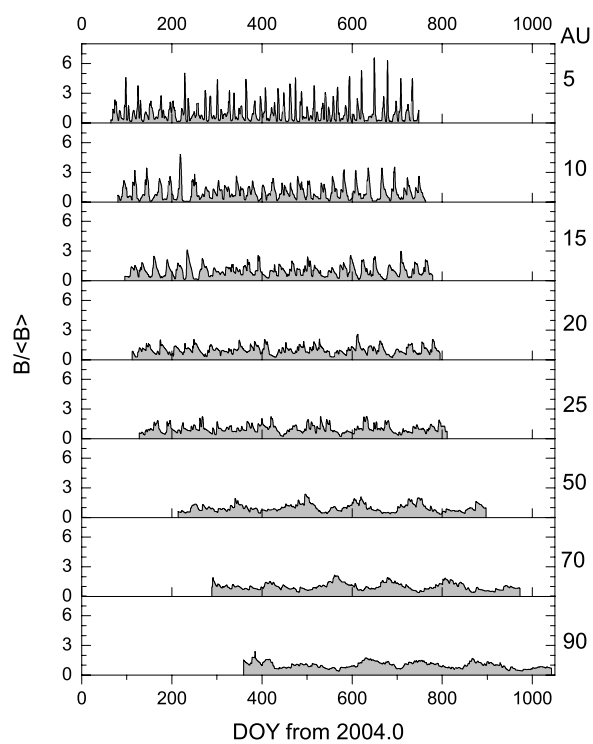

Figure 9. Predicted profiles of B/⟨B⟩ from 5 to 90 AU.

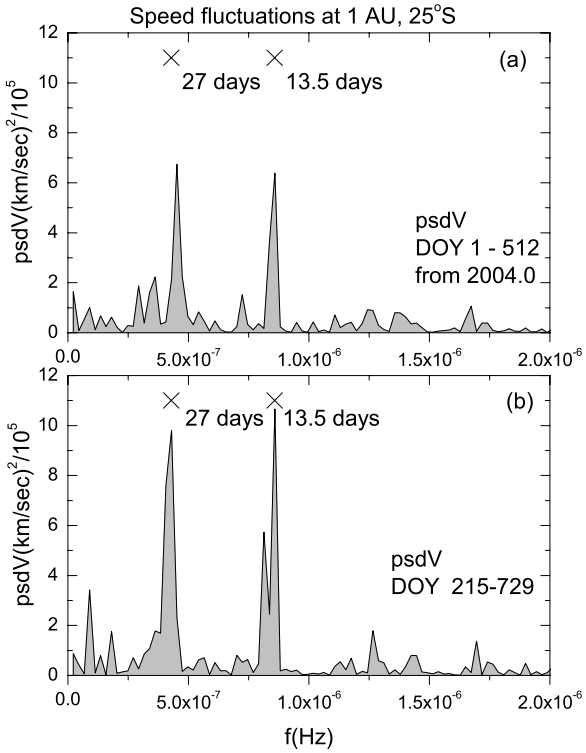

Figure 10. Power spectral density of the speed fluctuations at 1 AU at 25°S (a) from DOY 1-512 from DOY 1, 2004 and (b) from DOY 215–729.

pletely by 10 AU, leaving only a vestige of the corotating streams at 15 and 20 AU.

[47] At 5 AU, the spectrum of B shows two weak peaks of comparable magnitude at ≈26 days and ≈13 days (Figure 11), whereas at 1 AU there were no peaks in the spectrum of B, since B was assumed to be constant there. The spectral peaks of B at 5 AU are related to enhancements in B in interaction regions that were produced by the steepening of the corotating streams between 1 and 5 AU. At 10 AU the model predicts a strong peak at ≈26 days in the spectrum of fluctuations in B. This peak was produced by the coalescence of neighboring interactions to form MIRs between 1 AU and 10 AU, leaving 1 MIR per solar rotation at 10 AU. The MIRs damped appreciably between 10 and 15 AU, and no significant peak in the spectrum of B remained at 20 AU.

5.4. Radial Evolution of the Standard Deviation of V and B

[48] The radial evolution of the amplitudes of the large-scale fluctuations in B(t) and V(t) is summarized by the radial variations of standard deviations of daily averages of $B/\langle B\rangle(t)$ and V(t). The predicted $SD(B/\langle B\rangle)$ and SD(V) as a function of R, based on our solar boundary conditions, are shown in Figures 12a and 12b, respectively.

[50] The plot of SD(V) versus R in Figure 12b has a maximum at 5 AU and decays nearly exponentially with an e-folding scale of ≈14 AU to an asymptotic value of 25.4 km/s beyond ≈40 AU. This form of the radial variation of SD(V) was predicted by *Burlaga et al.* [2003a] for the speed associated with corotating streams predicted using the same equations but with the 1995 WIND boundary conditions. The SD(V) of the latter predictions are shown by the dashed curves in Figure 12b. The predicted radial variation of SD(V) is similar for the two types of boundary conditions, although the values of SD(V) are higher beyond 40 AU for the 1995 WIND boundary conditions than for our solar boundary conditions during 2004/2005. The predicted radial variation of SD(V) between 1 and 35 AU is similar to that reported by *Richardson et al.* [1996] for V2 observations made between 1 and ≈35 AU. *Wolfe* [1972]

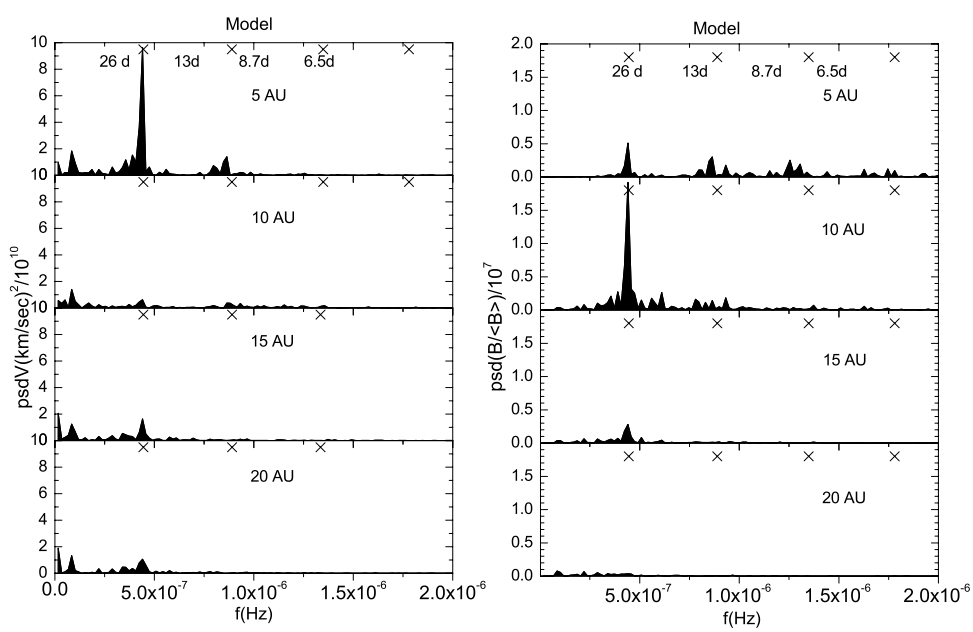

Figure 11. (left panels) Power spectral density of the speed fluctuations predicted at 5, 10, 15, and 20 AU. (right panels). Power spectral density of the fluctuations in $B/\langle B\rangle$ predicted at 5, 10, 15, and 20 AU.

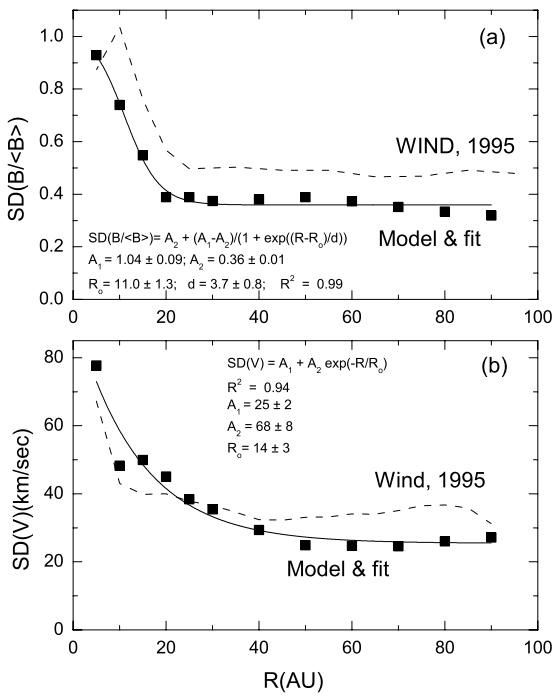

Figure 12. (a). The solid squares show SD(B/⟨B⟩) versus distance between 5 and 90 AU computed from the model of C. Wang with the boundary condition discussed in this paper for 2004–2005. The solid curve is a best fit of an exponential decay curve, shown in the figure together with the parameters of the fit. The dashed curve is the variation of SD(B/⟨B⟩ computed with the model of C. Wang using hour averages of WIND 1995 data as boundary conditions. (b). The solid squares show SD(V) versus distance between 5 and 90 AU computed from the model of C. Wang with the boundary condition discussed in this paper for 2004–2005. The solid curve is a best fit of an exponential decay curve, shown in the figure together with the parameters of the fit. The dashed curve is the variation of SD(B/⟨B⟩) computed with the model of C. Wang using hour averages of WIND 1995 data as boundary conditions.

was the first to observe the damping of streams with increasing distance from the Sun. We cannot determine the extent to which the quantitative differences between the two models are the result of considering different solar cycles or different types of data used for the inner boundary conditions.

[51] The SD(B/⟨B⟩) versus R predicted using our solar boundary conditions is maximum at 5 AU, decays between 5 and 20 AU, and remains constant between 20 and 90 AU. A similar radial variation of SD(B/⟨B⟩) was predicted by *Burlaga et al.* [2003b] for the magnetic field associated with corotating streams using the same equations but with the WIND 1995 boundary conditions. The latter predictions are shown by the dashed curves in Figure 12a. The radial variation predicted with the two types of boundary conditions is qualitatively the same. Both models predict a transition at ≈20 AU from weakening CMIRs to a constant level of random fluctuations. The model with the 1995 WIND boundary conditions predicts the largest fluctuations at 10 AU and a plateau of SD(B/⟨B⟩) ≈0.48 from 20 to 90 AU, whereas the model with the our solar boundary conditions predicts a peak at 10 AU AU and SD(B/⟨B⟩)≈0.36 from 20 to 90 AU.

6. Summary and Discussion

[52] This paper examines the daily averages of Voyager 2 (V2) observations of the magnetic field strength B, speed, V, and density N made as a function of time from 75.30 to 81.57 AU at heliographic latitudes between −25.7°S and −27.1°S during 2005 and 2006. These observations were interpreted using a model based on the 1-D time dependent MHD equations of C. Wang and a new method to determine the inner boundary conditions. The paper includes a comparison of 1) the observed and predicted trends of V(t), 2) the observed and predicted distributions of B, V, N, and NV^2 at V2, and 3) the predicted radial evolution of B(t) and V(t) between 1 AU and 90 AU computed using our solar boundary conditions.

[53] The trend in the speed profile observed by V2 during 2005 and 2006 (Figure 6) is characterized by 1) relatively homogeneous fluctuations about an average speed of ≈418 km/s during 2005.0, 2) a shock on DOY 59–60, 2006 followed by a MIR from DOY 60 to ∼100, 2006, and 3) higher speeds during the remainder of 2006. We do not consider the shock and flow system in this study. The model predicts an 'average' profile with approximately a constant speed during 2005, a jump in speed at ∼DOY 56, 2006, and a constant speed throughout the rest of 2006. The predicted speeds before and after the jump are ≈7% higher than observed.

[54] The speed profile observed by V2 has a jump-ramp structure. This form of the fluctuations in speeds is predicted, but the predicted amplitude of fluctuations is somewhat larger than the observed amplitude. The SD of the predicted distribution of V is 20 ± 3 km/s, compared to SD = 10 ± 2 km/s at V2 (excluding the shock flow).

[55] The distribution of log(B/⟨B⟩) observed by V2 during 2005 by V2 is Gaussian, indicating a lognormal distribution of B/⟨B⟩ (Figure 2a). The observed distribution of V is consistent with a Gaussian distribution within the uncertainties (Figure 2b). The model predicts both the observed lognormal distribution of B and the Gaussian distribution of V. The standard deviation of the predicted distribution of log(B/⟨B⟩) is SD = 0.16 ± 0.07 nT, consistent with SD = 0.17 ± 0.02 nT observed at V2. The SD of the observed speed distribution is twice as large as that predicted.

[56] The predicted distributions of log(N) and $\log(NV^2)$ are not Gaussian, in contrast to the Gaussian distributions observed by V2. This result might reflect the inadequacy of our solar boundary conditions, particularly our assumption that N and T can be derived from the speed on the inner boundary.

[57] The radial evolution of the profiles of V(t) and B(t) between 1 AU and 90 AU was computed using the model of C. Wang and our solar boundary conditions. Since these boundary conditions depend on V, which was computed from 3-D solar observations, it is possible to compute the radial variation of V and B beyond 1 AU using the model of Chi Wang (or better, a 3-D MHD model) with the solar boundary conditions for each of a broad range of latitudes and thereby build a 3-D model of the large-scale fluctua-

tions in V and B. However, this paper considers only the radial evolution of V(t) and B(t) at the particular latitude of 25.5°S, approximately the latitude of V2 during 2005. This restriction allows us to examine how the fluctuations observed by V2 developed, while providing a comparison with earlier models of the radial evolution computed with the same equations but using the WIND 1995 boundary conditions.

[58] The radial evolution of large-scale fluctuations of V(t) and B(t) predicted with the solar boundary conditions introduced in this paper are qualitatively the same as those derived from the same equations with the WIND 1995 boundary conditions [*Burlaga et al.*, 2003a, 2003b, respectively]. Both models are consistent with the conceptual picture of *Burlaga* [1983]. Pairs of fast recurrent streams, introduced at 1 AU in the "stream zone", merge between 1 and 5 AU to form compound streams and corotating MIRs in the "CMIR zone" between ≈5 and 15 AU. The fluctuations decay in the "wave interaction zone" beyond 20 AU.

[59] The spectrum of speed fluctuations on the inner boundary at 1 AU during 2004 shows 2 peaks of essentially the same magnitude, one at the solar rotation period (27 days) and the other at ≈13.5 days (two corotating streams per solar rotation). At 5 AU, the predicted spectrum of V shows a single strong peak at ≈26 days and only a weak remnant of a peak at 13 days. The spectral change is consistent with the conceptual model discussed above.

[60] Since we assumed a constant B at 1 AU, there are no peaks in the spectrum of B at 1 AU. At 5 AU, the predicted spectrum of B shows two weak peaks of comparable magnitude at ≈26 days and ≈13 days related to corotating interaction regions. At 10 AU, in the wave interaction zone, the model predicts a strong peak in the spectrum of fluctuations in B that was produced by the coalescence of neighboring interaction regions to form 1 MIR per solar rotation at 10 AU. The MIRs damped appreciably between 10 and 20 AU.

[61] The radial variations of SD(V) and SD(B/⟨B⟩) predicted with our solar boundary conditions are qualitatively the same as those predicted by the same equations with the WIND 1995 boundary conditions based on observations made at 1 AU during 1995. Both models predict 1) a rapid decay of the SD of the speed fluctuations, approaching a nearly constant value beyond ≈40 AU, and 2) a transition at ≈20 AU from weakening CMIRs identified as regions of high B) to a constant level of random fluctuations.

[62] There are quantitative differences in the results predicted by the model with our solar boundary conditions and the model with the WIND 1995 boundary conditions. We cannot determine the extent to which the quantitative differences between the two approaches are the result of considering different solar cycles, different types of data used for the inner boundary conditions, and latitudinal variations However, the important point is that the radial evolution of large-scale magnetic field strength fluctuations predicted by the model with our 3-D solar boundary conditions are qualitatively the same as with the WIND 1995 boundary conditions in the ecliptic plane. This result suggests the feasibility of predicting the global state of the heliosphere from solar observations and suitable 3-D MHD models.

[63] While the solar boundary conditions introduced in this paper offer the advantage of specifying boundary conditions at all latitudes, they have the disadvantage that their resolution and accuracy are relatively low. The approximations used in our solar boundary conditions do not allow one to accurately compute 1) the distributions of increments if B(t) and V(t) at various scales, 2) the multifractal structure of B(t) and V(t), and the slope of the spectra of B(t) and V(t) at periods <13.5 days.

[64] Further work aimed providing improved boundary conditions (ideally based entirely on solar observations) and using more advanced models to compute the structure of the solar wind beyond 1 AU has the potential to provide the conditions needed to compute the properties of large-scale fluctuations throughout the 3-D heliosphere. Some suggestions for future studies are as follows:

[65] 1. We assumed that the speed at 1 AU is similar that on the source surface, with a correction for interactions between fast and slow flows made by averaging neighboring pixels. It would be preferable to use a dynamical model to compute the speed profile on the boundary at 1 AU. In this way stream steepening, which was not considered in our approximation, could be taken into account.

[66] 2. We used a 1-D model for flow beyond 1 AU, with solar boundary conditions on a curve at 26° S on the boundary at 1 AU. It is possible to use a 3-D dynamical model with solar boundary conditions on the spherical boundary surface at 1 AU (many curves at different latitudes) to determine the global structure of the solar wind beyond 1 AU.

[67] 3. We computed the speed and density on the boundary at 1 AU from the speed profile, using correlations between the density and temperature with speed. An important challenge for experimenters in the next decade is to determine the density and temperature a spherical boundary directly from solar observations.

[68] 4. The solar magnetic field observations used to derive the speeds at 1 AU in this paper were derived from observations made at earth. It should be possible measure the solar magnetic field on the "back-side" of the Sun as well, giving more accurate and complete global speed profiles.

[69] 5. Given an approximation to the 3-D structure of the "stationary" solar wind related to corotating streams, it should be possible to model the effect of evolving corotating streams and individual ejecta moving through these streams.

[70] **Acknowledgments.** The contribution of the NRL co-authors was supported by NASA and the Office of Naval Research. The work at M.I.T. was supported under NASA contract 959203 from JPL to MIT and at Caltech by NASA contract NAS7-03001. C. Wang is grateful to the grant NNSFC 40325010. N. F. Ness appreciates partial support by NASA grant NNX06AG99G to CUA. This work was also supported in part by the International Collaboration Research Team Program of the Chinese Academy of Sciences.

[71] Wolfgang Baumjohann thanks Bala Poduval and Gary Zank for their assistance in evaluating this paper.

References

Arge, C. N., and V. J. Pizzo (2000), Improvement in the prediction of solar wind conditions using near-real time solar magnetic field updates, *J. Geophys. Phys.*, *105*(A5), 10,465–10,479.

Behannon, K. W., M. H. Acuna, L. F. Burlaga, R. P. Lepping, N. F. Ness, and F. M. Neubauer (1977), Magnetic-field experiment for Voyager-1 and Voyager-2, *Space Sci. Rev.*, *21*(3), 235–257.

Bridge, H. S., J. W. Belcher, R. J. Butler, A. J. Lazarus, A. M. Mavretic, J. D. Sullivan, G. L. Siscoe, and V. M. Vasyliunas (1977), The plasma experiment on the 1977 Voyager mission, *Space Sci. Rev.*, *21*, 259–287.

Burlaga, L. F. (1983), Corotating pressure waves without fast streams in the solar wind, *J. Geophys. Phys.*, *88*, 6085–6094.
Burlaga, L. F. (1984), MHD processes in the outer heliosphere, *Space. Sci. Rev.*, *39*(3–4), 255–316.
Burlaga, L. F. (1995), *Interplanetary Magnetohydrodynamics*, Oxford Univ. Press, New York.
Burlaga, L. F. (2001), Lognormal and multifractal distributions of the heliospheric magnetic field, *J. Geophys. Res.*, *106*(A8), 15,917–15,927.
Burlaga, L. F., and W. H. Mish (1987), Large-scale fluctuations in the interplanetary medium, *J. Geophys. Res.*, *92*(A2), 1261–1266.
Burlaga, L., and K. Ogilvie (1970a), Magnetic and thermal pressures in the solar wind, *Sol. Phys.*, *15*, 61.
Burlaga, L., and K. Ogilvie (1970b), Heating of the solar wind, *Astrophys. J.*, *159*, 659.
Burlaga, L. F., V. Pizzo, A. Lazarus, and P. Gazis (1985), Stream dynamics between 1 AU and 2 AU-a comparison of observations and theory, *J. Geophys. Res.*, *90*(A8), 7377–7388.
Burlaga, L. F., N. F. Ness, and F. B. McDonald (1987), Large-scale fluctuations in B between 13 AU and 25 AU and their effects on cosmic-rays, *J. Geophys. Res.*, *92*, 13,647–13,652.
Burlaga, L. F., W. H. Mish, and D. A. Roberts (1989), Large-scale fluctuations in the solar wind at 1 AU: 1978–1982, *J. Geophys. Res.*, *94*, 177.
Burlaga, L. F., N. F. Ness, J. D. Richardson, and R. P. Lepping (2001), The Bastille Day shock and merged interaction region at 63 AU: Voyager 2 observations, *Sol. Phys.*, *204*(1–2), 399–410.
Burlaga, L. F., C. Wang, J. D. Richardson, and N. F. Ness (2003a), Evolution of the multiscale statistical properties of corotating streams from 1 to 95 AU, *108*(A7), 1305, doi:10.1029/2003JA009841.
Burlaga, L. F., C. Wang, J. D. Richardson, and N. F. Ness (2003b), Evolution of magnetic fields in corotating interaction regions from 1 to 95 AU: Order to chaos, *Ap. J.*, *590*(1), 554–566.
Burlaga, L. F., C. Wang, J. D. Richardson, and N. F. Ness (2003c), Large-scale magnetic field fluctuations and development of the 1999–2000 global merged interaction region: 1-60 AU, *Astrophys. J.*, *585*(2), 1158–1168.
Burlaga, L. F., C. Wang, and N. F. Ness (2003d), A model and observations of the multifractal spectrum of the heliospheric magnetic field strength fluctuations near 40 AU, *Geophys. Res. Lett.*, *30*(10), 1543, doi:10.1029/2003GL016903.
Burlaga, L. F., N. F. Ness, C. Wang, J. D. Richardson, F. B. McDonald, and E. C. Stone (2005), A transition to fast flows and its effects on the magnetic fields and cosmic rays observed by Voyager 2 near 70 AU, *Astrophys. J.*, *618*, 1074–1078.
Burlaga, L. F., A. Viñas, and C. Wang (2007), Tsallis distributions of magnetic field strength variations in the heliosphere: 5 to 90 AU, *J. Geophys. Res.*, *112*, A07206, doi:10.1029/2006JA012213.
Holzer, T. E. (1972), Interaction of the solar wind with the neutral component of the interstellar gas, *J. Geophys. Res.*, *77*, 5407.
Hundhausen, A. J. (1972), *Coronal Expansion and Solar Wind*, Springer-Verlag, New York.
Hundhausen, A. J. (1977), An interplanetary view of coronal holes, in *Coronal Holes and High Speed Wind Streams*, edited by J. B. Zirker, pp. 225–329, Colo. Assoc. Univ. Press, Boulder, Colo.
Isenberg, P. A. (1986), Interaction of the solar wind with interstellar neutral hydrogen: 3-Fluid model, *J. Geophys. Res.*, *91*(A9), 9965–9972.
Lepping, R., et al. (1995), The Wind magnetic field investigation, *Space Sci. Rev.*, *71*, 207–229.
Levine, R. H., M. D. Altschuler, and J. W. Harvey (1977), Solar sources of interplanetary magnetic-field and solar-wind, *J. Geophys. Phys.*, *82*(7), 1061–1065.
Lopez, R. E., and M. P. Freeman (1986), The solar wind proton temperature-velocity relation, *J. Geophys. Phys.*, *91*, 1701.
McComas, D. J., et al. (1998), Solar wind electron proton alpha monitor (SWEPAM) for the Advanced Composition Explorer, *Space Sci. Rev.*, *86*, 563.
Neugebauer, M., and C. W. Snyder (1966), Mariner 2 observations of the solar wind 2: Average properties, *J. Geophys. Res.*, *71*, 4469.
Ogilvie, K., et al. (1995), SWE, A comprehensive plasma instrument for the Wind spacecraft, *Space Sci. Rev.*, *71*, 55–77.
Poduval, B., and X. P. Zhao (2004), Discrepancies in the prediction of solar wind using potential field source surface model: An investigation of possible sources, *J. Geophys. Res.*, *109*(A8), A08102, doi:10.1029/2004JA010384.
Rice, W. K. M., and G. P. Zank (1999), Shock propagation in the outer heliosphere: 2. Pickup ions and MHD, *J. Geophys. Res.*, *104*, 12,563–12,575.
Richardson, J. D., and C. Wang (2005), Voyager observations of interplanetary shocks. *The Physics of Collisionless Shocks*, G. Li, G. P. Zank, C. T. Russell eds., 278–282, AIP Conference Proceedings 781.
Richardson, J. D., J. W. Belcher, A. Lazarus, and K. Paularena (1996), Statistical properties of the solar wind, in *Solar Wind Eight*, edited by D. Winterhalter et al., AIP Conf. Proc., 382, 483–486.
Richardson, J. D., C. Wang, and L. F. Burlaga (2003), Correlated solar wind speed, density, and magnetic field changes at Voyager 2, *Geophys. Res. Lett.*, *30*(23), 2207, doi:10.1029/2003GL018253.
Richardson, J. D., Y. Liu, C. Wang, D. J. McComas, E. C. Stone, A. C. Cummings, L. F. Burlaga, M. H. Acuna, and N. F. Ness (2006), Source and consequences of a large shock near 79 AU, *Geophys. Res. Lett.*, *33*, L23107, doi:10.1029/2006GL027983.
Schatten, K. H., J. M. Wilcox, and N. F. Ness (1969), A model of the interplanetary and coronal magnetic fields, *Sol. Phys.*, *6*, 442–445.
Schwenn, R., M. Montgomery, H. Rosenbauer, H. Miggenreiter, K. Mühlhäuser, S. Bame, W. Feldman, and R. T. Hansen (1978), Direct observations of the latitudinal extent of a high-speed stream in the soar wind, *J. Geophys. Phys.*, *83*(A3), 1011.
Sheeley, N. R., Jr., Y.-M. Wang, and J. L. Phillips (1997), Near-Sun Magnetic Fields and the Solar Wind, in J. R. Jokipii, M. S. Giampapa, and C. P. Sonett (eds.), Cosmic Winds and the Heliosphere, Univ. Arizona Press, 459.
Wang, C., and J. D. Richardson (2001a), Energy partition between solar wind protons and pickup ions in the distant heliosphere: A three-fluid approach, *J. Geophys. Res.*, *106*(A12), 29,401–29,408.
Wang, C., and J. D. Richardson (2001b), Voyager 2 observations of helium abundance enhancements from 1-60 AU, *J. Geophys. Res.*, *106*(A4), 5683–5692.
Wang, Y. M., and N. R. Sheeley Jr. (1990), Solar-wind speed and coronal flux-tube expansion, *Ap. J.*, *355*(2), 726.
Wang, Y. M., and N. R. Sheeley Jr. (1992), On potential-field models of the solar corona, *Astrophys. J.*, *392*(1), 310–319.
Wang, Y. M., and N. R. Sheeley Jr. (2006), Sources of the solar wind at Ulysses during 1990–2006, *Astrophys. J.*, *653*, 708–718.
Wang, Y. M., N. R. Sheeley Jr., J. L. Phillips, and B. E. Goldstein (1997), Solar wind stream interactions and the wind speed-expansion factor relationship, *Astrophys. J.*, *488*(1), L51.
Wang, C., J. D. Richardson, and L. F. Burlaga (2001), Propagation of the Bastille Day 2000 CME shock in the outer heliosphere, *Sol. Phys.*, *204*(1–2), 411–421.
Whang, Y. C. (1991), Shock interactions in the outer heliosphere, *Space Sci. Rev.*, *57*, 339–388.
Whang, Y. C., and L. F. Burlaga (1985), Evolution and interaction of interplanetary shocks, *J. Geophys. Res.*, *90*, 10,765.
Whang, Y. C., and L. F. Burlaga (1988), Evolution of recurrent solar wind structures between 14 AU and the termination shock, *J. Geophys. Res.*, *93*, 5446–5460.
Whang, Y. C., L. F. Burlaga, N. F. Ness, and C. W. Smith (2001), The Bastille Day shocks and merged interaction region, *Sol. Phys.*, *204*(1-2), 255–265.
Whang, Y. C., L. F. Burlaga, Y. M. Wang, and N. R. Sheeley (2003), Solar wind speed and temperature outside 10 AU and the termination shock, *Ap. J.*, *589*(1), 635–643.
Whang, Y. C., Y. M. Wang, N. R. Sheeley, and L. F. Burlaga (2005), Global structure of the out-of-ecliptic solar wind, *J. Geophys. Res.*, *110*, A03103, doi:10.1029/2004JA010875.
Wolfe, J. H. (1972), The large-scale structure of the solar wind, in *Solar Wind*, edited by C. P. Sonett, P. J. Coleman Jr., and J. M. Wilcox, NASA Spec. Publ., NASA SP-308, 170-201.
Zank, G. P. (1999), Interaction of the solar wind with the local interstellar medium: A theoretical perspective, *Space Sci. Rev.*, *89*, 413–688.
Zank, G. P., and H. L. Pauls (1997), Shock propagation in the outer heliosphere: 1. Pickup ions and gasdynamics, *J. Geophys. Res.*, *102*, 7037–7049.

M. H. Acũna, Solar System Exploration Division, NASA Goddard Space Flight Center, Greenbelt, MD 20771, USA.
L. F. Burlaga, NASA/Goddard Space Flight Center, Geospace Physics Laboratory, Code 673 Greenbelt, MD 20771, USA. (leonard.f.burlaga@nasa.gov)
N. F. Ness, Institute for Astrophysics and Computational Sciences, Catholic University of America, Washington, DC 20064, USA.
J. D. Richardson, Kavli Institute for Astrophysics and Space Research, Massachusetts, Institute of Technology, 37-655, Cambridge, MA, USA.
N. R. Sheeley, Jr. and Y.-M. Wang, Naval Research Laboratory, Washington, DC 20375, USA.
C. Wang, State Key Laboratory of Space Weather, Center for Space Science and Applied Research, Chinese Academy of Science, Beijing, P.O. Box 8701, China.